Vol 15 No 12, December 2006
1009-1963/2006/15(12)/2909-11

Chinese Physics

© 2006 Chin. Phys. Soc.
and IOP Publishing Ltd

Laser-phase determination methods and transfer equations for direct temporal structure measurements of atto- and femtosecond XUV pulses

Ge Yu-Cheng(葛愉成)†

Department of Technical Physics, Peking University, Beijing 100871, *China*

(Received 30 May 2005; revised manuscript received 31 May 2006)

In this paper the laser-phase determination methods and transfer equations are presented to directly reconstruct the detailed temporal structures of ultra-short extreme ultraviolet (xuv) pulses from the measured photoelectron energy spectra (PES). Each transfer equation includes one of PID (proportional-integral-differential) terms of PES. The intensity and instantaneous frequency of attosecond xuv can be retrieved from the integral term of PES. The intensity profiles of narrow bandwidth atto- and femtosecond xuvs can be rebuilt from the proportional and differential terms of PES respectively. The methods and equations may be used to improve time resolutions in measuring ultrashort pulses.

Keywords: laser-phase determination, transfer equation, temporal structure, photoelectron spectrum
PACC: 3365, 3280F, 3280, 3365C

1. Introduction

Since the successful experiment on the generation of 650- as (1as= 10^{-18} s) isolated extreme ultraviolet (xuv) pulses was reported,[1,2] direct and accurate measurement of the temporal profile of ultrashort xuv pulse is a popular topic when one probes electronic dynamics in atoms, molecules and solids.[3] Several methods were proposed to determine the pulse duration.[4−12] The best time resolution estimated so far is $\sim$ 100as or slightly less. Very recently, techniques to generate, measure and use 250as xuv pulses were reported.[13,14] However, most of these methods were designed to get only the pulse duration by using a previous assumption of the pulse shape. Many Chinese authors have studied the atomic ionization in a strong laser field and the dynamic mechanism of high-order harmonic generation (HHG).[15−18] On the other hand, measuring temporal structure of fs (1fs= 10^{-15} s) xuv or x-ray pulse is still a challenge. Two techniques to produce sub-picosecond pulses of synchrotron radiation are the phonon Bragg switchy[19,20] and the slicing of electron bunches in a storage ring.[21] Another one is the laser synchrotron x-ray source of 90° Thomson scattering.[22]

With the development of new-generation ultrashort light sources and ultra-fast measurements, it is very important to directly measure the frequency and intensity temporal distributions of ultrashort xuv or x-ray pulses with high time resolutions. In this paper, a set of new methods are developed which apply the PID (proportional integral differential) terms of photoelectron energy spectrum (PES) to directly reconstruct the temporal profiles of atto- and femtosecond xuv pulses. By using a cross correlation between a low frequency laser and a high frequency xuv, the excited PES is measured at 0° or 180° with respect to the linear laser polarization.[23−25]

This paper is organized as follows. Section 2 describes the methods of laser-phase determination and transfer equations. Section 3 presents the calculations and retrievals of the pulses. Section 4 summarizes the paper.

2. Laser-phase determination methods and transfer equations

2.1. Basic equations

The large difference in angular frequencies between xuv $\omega_{\rm X}$ and laser $\omega_{\rm L}$ naturally divides the two-colour ionization process into two steps: the electron

†E-mail: gyc@hep.pku.edu.cn

is instantaneously ionized from a gas atom via absorption of an atto- or femtosecond xuv photon and next it moves in the electric field of a femtosecond laser as a classical particle,[26] as shown in Fig.1.

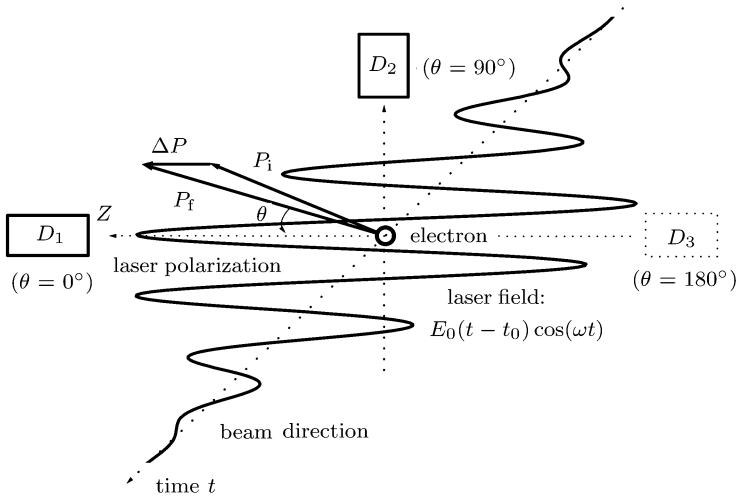


Fig.1. Electron movement in a laser field. D_1, D_2 and D_3 are electron energy spectrometers at $\theta = 0°$, $90°$ and $180°$ respectively, which are perpendicular to the laser beam direction.

As the laser leaves the interaction volume, the momentum or energy of the produced photoelectron will experience a shift that depends on the laser intensity and the carrier phase at the time of ionization. With the assumptions of $U_p \gg \hbar\omega_L$ (where U_p is the electron quiver energy in the laser field, i.e. the ponderomotive energy) and $\hbar\omega_X \gg I_p$, classical mechanics can be used.[27,28] The produced photoelectron has an initial kinetic energy $W_i = P_i^2/2m_e = \hbar\omega_X - W_b$, where m_e is the electron mass, W_b and P_i are the atomic ionization potential and the initial momentum respectively, in an arbitrary direction. The laser field is assumed to be $E_L(t) = E_a(t-t_0)\cos\omega_L t = E_0 F(t-t_0)\cos\omega_L t$, where E_0 is the maximum amplitude of the electric field, $E_a(t-t_0)$. $F(t-t_0)$ is the laser envelope peaked at the time $t = t_0$(fs), and $\Phi = \omega_L t_0$ is the laser carrier-envelope phase. In adiabatic limit $\mathrm{d}E_a/\mathrm{d}t \ll E_a\omega_L$, the equation for electron motion can be readily integrated. The final momentum shift of an electron released at the instant t along the laser polarization can be written as

$$\begin{aligned}\Delta P(t) =& -e\int_t^\infty E_L(t')\mathrm{d}t',\\ \approx& -\frac{eE_a(t-t_0)}{\omega_L}\sin\omega_L t,\\ =& -2\sqrt{m_e U_0}F(t-t_0)\sin\omega_L t, \qquad (1)\end{aligned}$$

where e is the electron charge. The time-dependent electron quiver energy,

$$U_p(t-t_0) = e^2E_a^2(t-t_0)/4m_e\omega_L^2 = U_0F^2(t-t_0),$$

where U_0 is the maximum value at $t = t_0$.

The final energy of a photoelectron is $(\boldsymbol{P}_i + \Delta\boldsymbol{P})^2/2m_e$, which can be written as

$$\begin{aligned}W_f(t,\theta) =& W_i(t) + 2U_p(t-t_0)\sin^2\omega_L t\cos 2\theta\\ &+ \{8U_p(t-t_0)[W_i(t) - 2U_p(t-t_0)\\ &\cdot\sin^2\omega_L t\sin^2\theta]\}^{1/2}\sin\omega_L t\cos\theta, \qquad (2)\end{aligned}$$

where $W_i(t)$ is the initial kinetic energy of the photoelectron at the birth time t, and θ is the angle between the final momentum and the laser polarization. Particularly, $W_{90°}(t)$, $W_{0°}(t)$ and $W_{180°}(t)$ are defined as the birth-time-dependent final energies of the photoelectrons observed at $\theta = 90°$, $0°$ and $180°$, respectively. According to Eq.(2), they read

$$W_{90°}(t) = W_i(t) - 2U_0F^2(t-t_0)\sin^2\omega_L t, \qquad (3)$$

$$\begin{aligned}W_{0°}(t) =& W_i(t) + 2U_0F^2(t-t_0)\sin^2\omega_L t\\ &+ \sqrt{8U_0W_i}\,F(t-t_0)\sin\omega_L t, \qquad (4)\end{aligned}$$

$$\begin{aligned}W_{180°}(t) =& W_i(t) + 2U_0F^2(t-t_0)\sin^2\omega_L t\\ &- \sqrt{8U_0W_i}\,F(t-t_0)\sin\omega_L t. \qquad (5)\end{aligned}$$

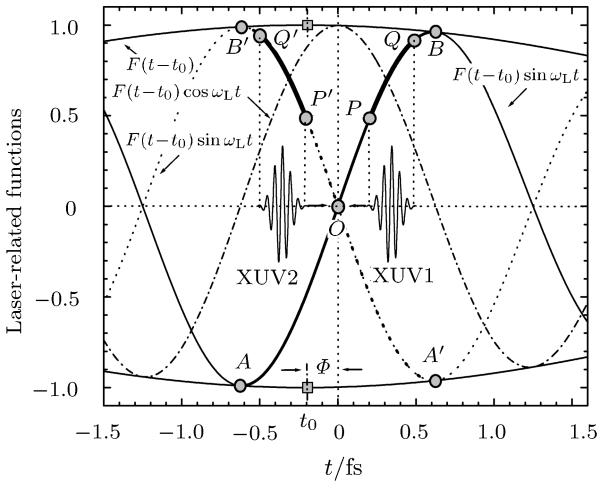


Fig.2. The laser-related functions: $F(t-t_0)$, $F(t-t_0)\cos\omega_L t$, $F(t-t_0)\sin\omega_L t$ and $-F(t-t_0)\sin\omega_L t$. XUV1 and XUV2 are the same xuv pulse located at different temporal positions ($t \geq 0$ and $t \leq 0$) within half a laser optical cycle.

According to Eq.(2), $\mathrm{d}W_\mathrm{f}(t,\theta)/\mathrm{d}\theta = 0$ at $\theta = 0°$ and 180°. This means that the photoelectron spectrometer set at $\theta = 0°$ or 180° can work with a big collection angle than that at $\theta = 90°$. When $W_\mathrm{i}(t)$ has a narrow bandwidth ΔW, the differential, $\mathrm{d}W_{0°}(t)$, can be written as

$$\begin{aligned}\mathrm{d}W_{0°}(t) &= [1+\sqrt{2U_0/W_\mathrm{i}}F(t-t_0)\sin\omega_L t]\mathrm{d}W_\mathrm{i}(t),\\ &\approx \mathrm{d}W_\mathrm{i}(t)\end{aligned}$$

$$\approx \Delta W \ \ (2U_0 \ll W_\mathrm{i}, \Delta W \ll W_\mathrm{i}). \qquad (6)$$

Equation (6) tells us that the spectral broadening of the PES depends on the pulse bandwidth.

In the following subsections, we focus on determining the electron birth time t or the laser-related carrier phase $\omega_L t$ from PES for atto- and femtosecond xuv measurements.

2.2. Laser-phase determination method and transfer equation for attosecond XUV pulse measurement

Usually, for an attosecond xuv pulse, e.g. one produced by HHG, its temporal structure includes both frequency and intensity temporal distributions. The laser-related functions, $F(t-t_0)$, $F(t-t_0)\cos\omega_L t$, as well as $F(t-t_0)\sin\omega_L t$ and $-F(t-t_0)\sin\omega_L t$, are shown in Fig. 2. XUV1 or XUV2 represents an attosecond xuv pulse being cross-correlated to half a laser optical cycle. For the photoelectrons moving at $\theta = 0°$, $W_{0°}^\mathrm{L}$ and $W_{0°}^\mathrm{H}$ are defined as the final energies measured with low and high laser intensities, S_1 and S_2 (corresponding to low and high ponderomotive energies U_0^L and U_0^H) respectively. The birth time t (or the laser-phase $\omega_L t$) and its initial kinetic energy $W_\mathrm{i}(t)$ satisfy the following equations:

$$F(t-t_0)\sin\omega_L t = \frac{\sqrt{W_{0°}^\mathrm{H}}-\sqrt{W_{0°}^\mathrm{L}}}{\sqrt{2U_0^\mathrm{H}}-\sqrt{2U_0^\mathrm{L}}}, \qquad W_\mathrm{i}(t) = \left[\sqrt{W_{0°}^\mathrm{H}}-\sqrt{2U_0^\mathrm{H}}\cdot\frac{\sqrt{W_{0°}^\mathrm{H}}-\sqrt{W_{0°}^\mathrm{L}}}{\sqrt{2U_0^\mathrm{H}}-\sqrt{2U_0^\mathrm{L}}}\right]^2. \qquad (7)$$

Similarly, for a photoelectron moving at $\theta = 180°$, $W_{180°}^\mathrm{L}$ and $W_{180°}^\mathrm{H}$ are defined as the final energies measured with different laser intensities S_1 and S_2, its birth time and the initial energy satisfy the following equations:

$$F(t-t_0)\sin\omega_L t = -\frac{\sqrt{W_{180°}^\mathrm{H}}-\sqrt{W_{180°}^\mathrm{L}}}{\sqrt{2U_0^\mathrm{H}}-\sqrt{2U_0^\mathrm{L}}}, \qquad W_\mathrm{i}(t) = \left[\sqrt{W_{180°}^\mathrm{H}}-\sqrt{2U_0^\mathrm{H}}\cdot\frac{\sqrt{W_{180°}^\mathrm{H}}-\sqrt{W_{180°}^\mathrm{L}}}{\sqrt{2U_0^\mathrm{H}}-\sqrt{2U_0^\mathrm{L}}}\right]^2. \qquad (8)$$

Equations (7) and (8) are the bases of the laser-phase determination method for attosecond measurement. The key problem is how to determine the energies $W_{0°}^\mathrm{L}$ and $W_{0°}^\mathrm{H}$ (or $W_{180°}^\mathrm{L}$ and $W_{180°}^\mathrm{H}$) which correspond to the same laser carrier phase.

The laser-assisted photo-ionization production can be described by a cross-section, $\sigma(\hbar\omega_\mathrm{X})$, a photon-energy function called as the excitation function. The PES, $n(W)$, is defined as the number of photoelectrons per unit energy. For an initial intensity profile $f_0(t)$ of the xuv pulse, as shown in Fig.3(a), the number of photoelectrons measured at energy W_1 within a small interval $\mathrm{d}W_1$ is proportional to the xuv photons at the instant $t = t_1$ within a small interval $\mathrm{d}t_1$,

$$g\eta\rho\sigma(\hbar\omega_\mathrm{X})\cdot f_0(t_1)\mathrm{d}t_1 = n(W_1)\mathrm{d}W_1, \qquad (9)$$

where W_1 is the photoelectron energy satisfying $\hbar\omega_\mathrm{X} = W_\mathrm{i}(t_1) + W_\mathrm{b}$, g is a constant geometric factor of the spectrometer, and ρ is the atomic density

of the active gas, η is the electron detecting efficiency at the energy W_1. Usually, η is an approximate constant for energies concerned. Moving $g\eta\rho\sigma(\hbar\omega_{\rm X})$ to the right-hand side of Eq.(9), and integrating the left-hand side from $t_1 = t_s$ (the pulse starting time) to t and the right-hand side from the corresponding spectral position $W_1 = W_{\min}$ to W, we have

$$\int_{t_s}^{t} f_0(t_1)\mathrm{d}t_1 = \int_{W_{\min}}^{W} \frac{1}{g\eta\rho\sigma(\hbar\omega_{\rm X})}\cdot n(W_1)\mathrm{d}W_1. \quad (10)$$

Clearly, the integral of the left side of Eq.(10) is related only to time t, but the corresponding spectral position W is variable (if $t \neq 0$) when the laser intensity changes (see points Y and Z in Fig.3(a)). If the product $g\eta\rho\sigma(\hbar\omega_{\rm X})$ can be approximately set to be a constant for xuv photon energies within the bandwidth, another constant μ can be used instead of $1/g\eta\rho\sigma(\hbar\omega_{\rm X})$, and Eq.(10) can be written as

$$\int_{t_s}^{t} f_0(t_1)\mathrm{d}t_1 = \mu\int_{W_{\min}}^{W} n(W_1)\mathrm{d}W_1 \equiv \mu I(W). \quad (11)$$

Equation (11) can be used to determine the laser-phase of a photoelectron from two energy-integrated PES, $I(W)$, measured with two different laser intensities S_1 and S_2.

Figure 3(a) schematically shows the temporal distributions, $W_{\rm i}(t)$, $W^{\rm L}_{0^\circ}(t)$ and $W^{\rm H}_{0^\circ}(t)$. The latter two distributions are modulated from $W_{\rm i}(t)$ with different laser intensities at $\theta = 0^\circ$. Fig.3(b) plots their energy-integrals $I(W)$ (where μ is approximately set to 1 for simplicity). The photoelectrons generated at t_1 (see points Y and Z in Fig.3(a)) have the same phase and the same spectral value of $I(W)$ but different energy positions of the $n(W)$, e.g. $W^{\rm L}_{0^\circ}$ and $W^{\rm H}_{0^\circ}$ (see points Y and Z in Fig.3(b)) (or $W^{\rm L}_{180^\circ}$ and $W^{\rm H}_{180^\circ}$). With these energy values, both the birth time t and the initial kinetic energy $W_{\rm i}(t)$ of a photoelectron can be calculated by using Eqs.(7) or (8). Consequently, the instantaneous frequency is $[W_{\rm i}(t) + W_{\rm b}]/2\pi\hbar$. With the solutions of t, the energy-integrated spectrum $I(W)$ measured with high laser intensity S_2 can be converted to a temporal spectrum, $I(t) = I(W)$. Its time derivative, $f(t) = \mathrm{d}I(t)/\mathrm{d}t$, can be used to retrieve the initial intensity profile $f_0(t)$.

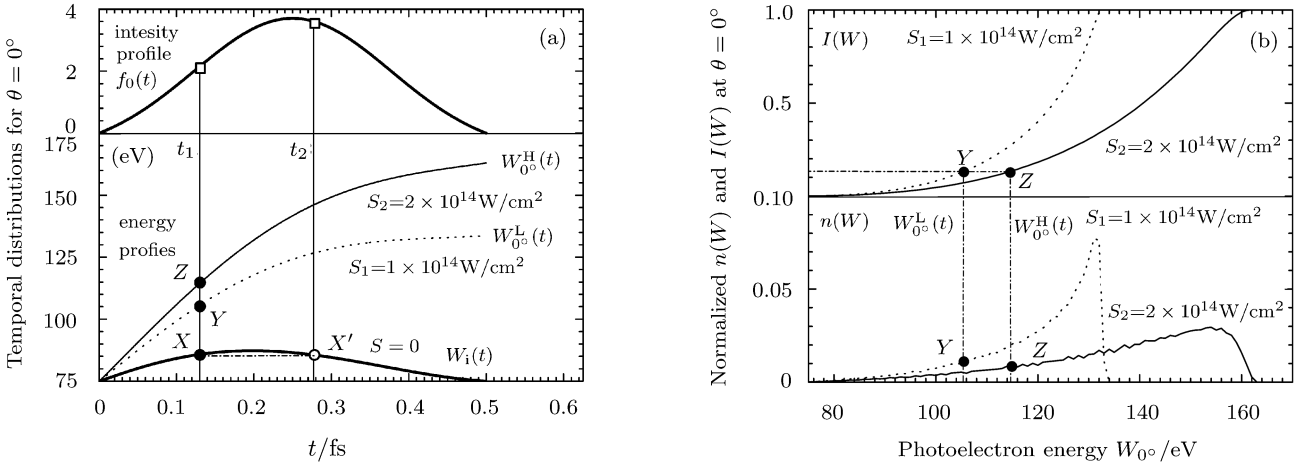


Fig.3. (a) The specified initial intensity and energy temporal profiles, $f_0(t)$ and $W_{\rm i}(t)$, starting at $t = 0$ for $\theta = 0^\circ$ measurement, as well as the modulated energy functions, $W^{\rm L}_{0^\circ}(t)$ and $W^{\rm H}_{0^\circ}(t)$. (b) The calculated and normalized energy spectra $n(W)$, and their energy-integrated spectra $I(W)$ with different laser intensities S_1 and S_2 for $\theta = 0^\circ$ measurements.

In the absence of laser, the photoelectrons released at different times t_1 and t_2 (see points X and X' in Fig.3(a)) have the same position on the energy spectrum (called phase-overlapping). With appropriate laser intensities, both new point Y and Z (modulated from the point X) have different energy positions without any phase-overlapping. In order to avoid phase-overlapping and obtain a continuously increasing line modulated from the momentum profile $P_{\rm i}(t)$, it is required that, $\mathrm{d}P(t)/\mathrm{d}t = \mathrm{d}P_{\rm i}(t)/\mathrm{d}t + 2\sqrt{m_{\rm e}U_0}\cdot\mathrm{d}[F(t-t_0)\sin\omega_{\rm L}t]/\mathrm{d}t \approx \mathrm{d}P_{\rm i}(t)/\mathrm{d}t + 2\omega_{\rm L}\sqrt{m_{\rm e}U_0}\cos\omega_{\rm L}t > 0$, i.e., $\sqrt{U_0} > [-\mathrm{d}P_{\rm i}(t)/\mathrm{d}t]/[2\omega_{\rm L}\sqrt{m_{\rm e}}\cos\omega_{\rm L}t]$. U_0 or laser peak intensity, S, is mainly determined by the maximum value of $[-\mathrm{d}P_{\rm i}(t)/\mathrm{d}t]/\cos\omega_{\rm L}t$ along the down-slope of $P_{\rm i}(t)$. This is also true for the energy profile $W_{\rm i}(t)$.

Usually, the laser intensity cannot be increased to very high levels because of measurement background. An alternative is to perform a $\theta = 180°$ measurement in which the xuv pulse is located at $t \le 0$ (denoted as t') and the PES is measured at $\theta = 180°$. Combining the data of $\theta = 0°$ and $180°$ measurements will give better retrievals of $W_{\rm i}(t)$ and $f(t)$. In addition, setting $t_s = 0$ fs, i.e. the start time of the xuv pulse for $\theta = 0°$ measurement, or the end time of the pulse for $\theta = 180°$ measurement, results in losing some frequency and intensity information near t_s due to weak modulation (where $\sqrt{W^{\rm H}_{0°}} - \sqrt{W^{\rm L}_{0°}}$ or $\sqrt{W^{\rm H}_{180°}} - \sqrt{W^{\rm L}_{180°}}$ has a very small value). Therefore it is suggested that the xuv pulse should be delayed (for $\theta = 0°$ measurement) or advanced (for $\theta = 180°$ measurement) for a small time.

2.3. Laser-phase determination method and transfer equation for narrow bandwidth attosecond XUV pulse measurement

For a narrow bandwidth attosecond xuv pulse, e.g. one produced by HHG and selected by a narrow bandwidth filter, the intensity structure and the temporal uncertainties at different times due to the bandwidth are concerned. An equivalence of Eq.(4) can be written as

$$\begin{aligned}\sin\omega_{\rm L}t &= \frac{\sqrt{W_{0°}} - \sqrt{W_{\rm i}}}{\sqrt{2U_0}F(t-t_0)} \\ &= \frac{\sqrt{m_{\rm e}\varepsilon_0 c}}{e}\cdot\frac{\omega_{\rm L}}{\sqrt{S}} \\ &\quad\cdot\frac{1}{F(t-t_0)}\cdot(\sqrt{W_{0°}} - \sqrt{W_{\rm i}}),\end{aligned} \tag{12}$$

where $W_{0°}$ is the photoelectron energy measured at $\theta = 0°$. With an iterating calculation, which approximately sets $W_{\rm i}$ to be the centre energy of xuv, the birth time t or the laser-phase $\omega_{\rm L}t$ of a photoelectron can be determined with $W_{0°}$. The narrower the xuv bandwidth is, the more accurate the phase determination is.

The shaded area in Fig.4(a) illustrates an attosecond xuv pulse being correlated to the carrier field within half a laser optical cycle (shown as a dotted curve $A'P'B'$ or a sinusoidal curve APB). $W_{0°}(t)$ is shown as a dash-dotted line in Fig.4(b). The highlighted curve APB in Fig.4(b) has the same phase range as that in Fig.4(a). If the temporal structure of this xuv pulse is $f(t)$, then the photoelectrons will populate along the energy axis from W_1 to W_2 (corresponding to the temporal range from a to b).

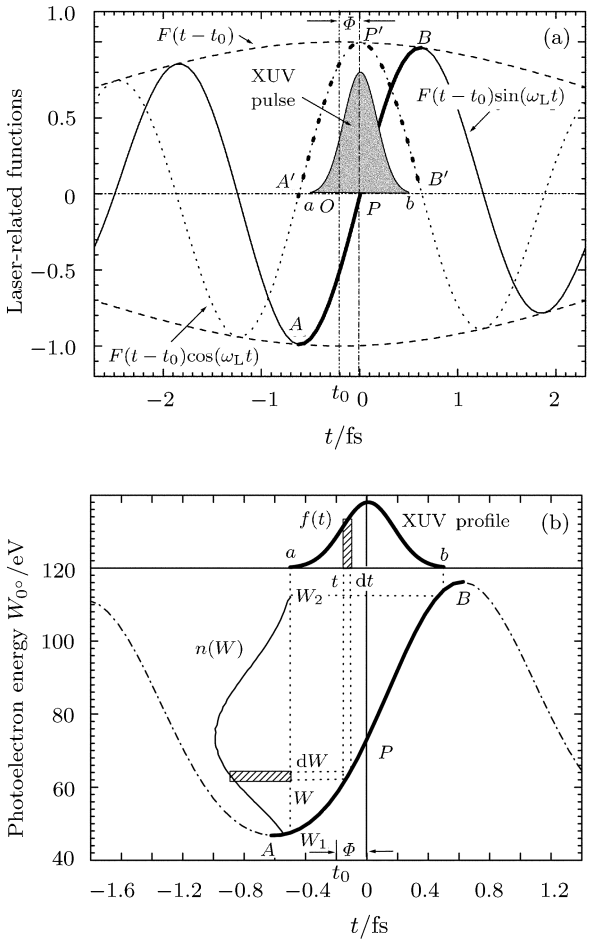


Fig.4. The laser-related functions: $F(t-t_0)$, $F(t-t_0)\cos\omega_{\rm L}t$ and $F(t-t_0)\sin\omega_{\rm L}t$. The shaded Gaussian-like profile illustrates the intensity distribution of an incident xuv pulse. (b) The derivation of transfer equation for narrow bandwidth attosecond xuv measurement at $\theta = 0°$.

According to Eq.(4),

$$\begin{aligned}\frac{{\rm d}W_{0°}(t)}{{\rm d}t} &= 2U_0[2F(t-t_0)\frac{{\rm d}F(t-t_0)}{{\rm d}t}\sin^2\omega_{\rm L}t \\ &\quad + 2\omega_{\rm L}F^2(t-t_0)\sin\omega_{\rm L}t\cos\omega_{\rm L}t] \\ &\quad + \sqrt{8U_0W_{\rm i}}\Big[\frac{{\rm d}F(t-t_0)}{{\rm d}t}\sin\omega_{\rm L}t \\ &\quad + \omega_{\rm L}F(t-t_0)\cos\omega_{\rm L}t\Big].\end{aligned} \tag{13}$$

Note that ${\rm d}F(t-t_0)/{\rm d}t \approx 0$ within half a laser optical cycle around $t = 0$ fs, and we can approximately simplify Eq.(13) to

$$\frac{{\rm d}W_{0°}(t)}{{\rm d}t} \approx \omega_{\rm L}\sqrt{8U_0W_{\rm i}}F(t-t_0)\cos\omega_{\rm L}t, \tag{14}$$

when $U_0 \ll 2W_{\rm i}$. With the same meanings of $n(W)$ and μ as those in Eq.(11), the temporal structure $f(t)$

can be calculated as

$$f(t) = \frac{\mathrm{d}W_{0^\circ}(t)}{\mathrm{d}t} \cdot \mu n(W), \tag{15}$$

or a more simplified form when $U_0 \ll 2W_\mathrm{i}$ as

$$f(t) \approx \omega_\mathrm{L}\sqrt{8U_0W_\mathrm{i}}\cdot F(t-t_0)\cos\omega_\mathrm{L}t \cdot \mu n(W). \tag{16}$$

Eq.(15) (with a complete calculation of Eq.(13) and Eq.(16) are transfer equations to calculate the unknown temporal structure $f(t)$ from a proportional term of the measured PES, $\mu n(W)$.

The temporal uncertainty or error-bar length Δt of the retrieved $f(t)$ due to the xuv bandwidth ΔW is

$$\Delta t = \frac{\Delta W}{|\mathrm{d}W_{0^\circ}(t)/\mathrm{d}t|}, \tag{17}$$

where $\mathrm{d}W_{0^\circ}(t)/\mathrm{d}t$ is calculated by using Eq.(13).

2.4. Transfer equations for narrow bandwidth femtosecond XUV pulse measurement

Different from an attosecond pulse, a femtosecond xuv pulse will be correlated to both laser carrier and its envelope. Since the duration τ of a femtosecond xuv pulse created by any way is much longer than the laser optical cycle T ($\tau \gg T$), the carrier-envelope phase Φ is unimportant and it can be set to 0 for a femtosecond or sub-picosecond laser. $W_{90^\circ}(t)$ is an oscillating curve which is plotted in Fig.5(a). The reversed bell-shaped curve, $W(t)$, is an envelope of the minimum values of $W_{90^\circ}(t)$,

$$W(t) = W_\mathrm{i} - 2U_\mathrm{p}(t). \tag{18}$$

In order to derive transfer equations, an approximately straight line is used instead of a continuously increasing/decreasing curve segment of $W_{90^\circ}(t) = W_\mathrm{i} - 2U_\mathrm{p}(t)\sin^2(\omega_\mathrm{L}t)$. As shown in Fig.5(a), the xuv temporal structure $f(t)$ has an intensity distribution from a to b. $a > 0$ ensures that the xuv pulse is correlated to the falling side of the laser pulse. Similar to the attosecond measurements, the number of electrons collected at energy W within a small energy interval $\mathrm{d}W$ is an integral of $f(t')$ with a factor $g\eta\rho\sigma(\hbar\omega_\mathrm{X})\cdot\mathrm{d}W/2U_0F^2(t')$ over time t' from a to t,

$$n(W)\mathrm{d}W = \int_a^t g\eta\rho\sigma(\hbar\omega_\mathrm{X})\cdot\frac{\mathrm{d}W}{2U_0F^2(t')}\cdot f(t')\mathrm{d}t'. \tag{19}$$

$\sigma(\hbar\omega_\mathrm{X})$ can be approximately set to be a constant for a narrow bandwidth femtosecond xuv or soft x-ray. The time t in Eq.(19) can be calculated from Eq.(18). Using a constant μ instead of $1/g\eta\rho\sigma(\hbar\omega_\mathrm{X})$, we can simplify Eq.(19) to

$$n(W) = \frac{1}{\mu}\int_a^t \frac{f(t')}{2U_0F^2(t')}\mathrm{d}t'. \tag{20}$$

Combining Eqs.(20) and (18) we have

$$\begin{aligned}\frac{\mathrm{d}n(W)}{\mathrm{d}W} &= \frac{\mathrm{d}n(W)}{\mathrm{d}t}\cdot\frac{1}{\mathrm{d}W(t)/\mathrm{d}t} \\ &= -\frac{1}{\mu}\cdot\frac{f(t)}{8U_0^2F^3(t)\mathrm{d}F(t)/\mathrm{d}t}.\end{aligned} \tag{21}$$

Thus $f(t)$ can be calculated from the energy-differential term of PES, $\mathrm{d}n(W)/\mathrm{d}W$, as follows:

$$\begin{aligned}&W = W_\mathrm{i} - 2U_0F^2(t), \\ &f(t) = -4\mu U_0^2F^2(t)\cdot\frac{\mathrm{d}F^2(t)}{\mathrm{d}t}\cdot\frac{\mathrm{d}n(W)}{\mathrm{d}W}.\end{aligned} \tag{22}$$

Two equations in Eq.(22) are transfer equations for $\theta = 90^\circ$ femtosecond measurement. The time t corresponding to the spectral position W can be solved from the first equation of Eq.(22), while the intensity profile $f(t)$ can be calculated from the second equation.

Note that $n(W)$ at $\theta = 0^\circ$ is almost the same as that at $\theta = 180^\circ$, and that it spans almost symmetrically below and above W_i (because the second term of Eq.(4) is much less than the third term when $U_0 \ll 2W_\mathrm{i}$), we can express the number of photoelectrons collected at energy W within an interval $\mathrm{d}W$

$$\begin{aligned}n(W)\mathrm{d}W = \frac{1}{2}\int_a^t &g\eta\rho\sigma(\hbar\omega_\mathrm{X}) \\ &\cdot\frac{\mathrm{d}W}{2\sqrt{8U_0W_\mathrm{i}}F(t')}\cdot f(t')\mathrm{d}t'.\end{aligned} \tag{23}$$

Similar to the derivation of Eq.(22), $f(t)$ can be calculated from the differential spectrum $\mathrm{d}n(W)/\mathrm{d}W$ (when $W > W_\mathrm{i}$) measured at $\theta = 0^\circ$ or 180° as follows:

$$\begin{aligned}&W = W_\mathrm{i} + 2U_0F^2(t) + \sqrt{8U_0W_\mathrm{i}}\cdot F(t), \\ &f(t) = 4\mu U_0[2W_\mathrm{i} + \sqrt{8U_0W_\mathrm{i}}\cdot F(t)] \\ &\qquad\cdot\frac{\mathrm{d}F^2(t)}{\mathrm{d}t}\cdot\frac{\mathrm{d}n(W)}{\mathrm{d}W}.\end{aligned} \tag{24}$$

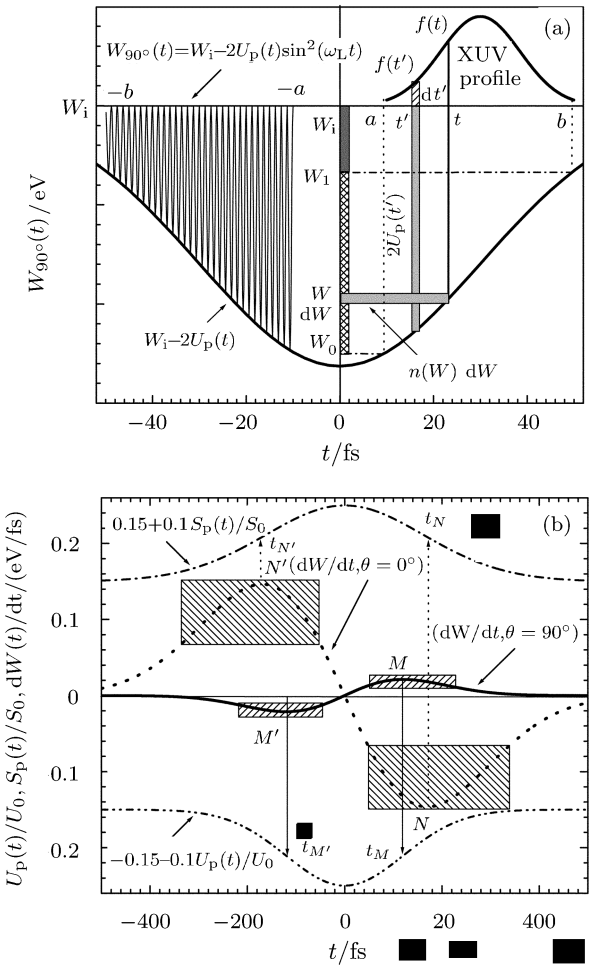


Fig.5. (a) The derivation of PES $n(W)$ at $\theta = 90°$. (b) The shapes of $U_p(t)/U_0$, $S_p(t)/S_0$ and $dW(t)/dt$ at $\theta = 90°$ and $0°$. The shaded areas refer to feasible measurement ranges.

For $\theta = 90°$ measurement, $U_p(t)/U_0$ describes the evolution of the photoelectron maximum energy down-shift, which is shown as a dash-dot-dotted line in Fig.5(b). For $\theta = 0°$ measurement,

$$S_p(t) \equiv W(t) - W_i = 2U_0F^2(t) + \sqrt{8U_0W_i}\cdot F(t) \qquad (25)$$

is defined as the maximum photoelectron energy up-shift, shown as a dash-dotted line in Fig.5(b), where $W(t)$ is the envelope of $W_{0°}(t)$. $S_0 = 2U_0 + \sqrt{8U_0W_i}$ is the maximum value of $S_p(t)$ at $t = 0$.

The curves of $dW(t)/dt$ calculated from the right-hand sides of the first equations of Eqs.(22) and (24) are shown in Fig.5(b). The plots show that $dW(t)/dt$ reach maximum absolute values at times t_M and $t_{M'}$ for $\theta = 90°$ measurement, and at t_N and $t_{N'}$ for $\theta = 0°$ measurement, respectively. The best linearity between dW and dt occurs around t_M, $t_{M'}$ or t_N, $t_{N'}$. Therefore, the measurement should be performed within the shaded areas in Fig.5(b), i.e. the xuv pulse should be temporally located around or even centred at $t_M(t_{M'})$ or $t_N(t_{N'})$.

The temporal uncertainty or error-bar length of the retrieved $f(t)$ at time t due to the xuv bandwidth ΔW is

$$\Delta t = \frac{\Delta W}{|dW(t)/dt|}, \qquad (26)$$

where

$$dW(t)/dt = -4U_0F(t)\cdot dF(t)/dt \qquad (27)$$

for $\theta = 90°$ measurement and

$$dW(t)/dt = [4U_0F(t) + \sqrt{8U_0W_i}]\cdot dF(t)/dt \qquad (28)$$

for $\theta = 0°$ measurement.

3. Numerical calculation

To illustrate this, Krypton is used as an active material. Its ionization potential W_b of 4p electron is 14 eV. A Gaussian-like shape of $F(t - t_0) = \exp[-4ln2\cdot(t-t_0)^2/\tau^2]$ is implemented for the laser envelope. For simplicity, the factors μ in transfer equations are set to be 1.

3.1. Frequency and intensity temporal profiles of an attosecond XUV pulse

We consider an attosecond xuv pulse which has a wide energy distribution from 89 to 101.3 eV. The photoelectron initial kinetic energy $W_i(t)$ will range from 75 to 87.3 eV. $W_i(t) = 74.8 + 115.8t - 145.6t^2 - 1029.5t^3 + 2329.8t^4 - 1226.5t^5$ (eV) and $f_0(t) = -0.63 + 4.33\exp[-2(t - 0.25)^2/0.26^2]$ are assumed as the initial photoelectron kinetic energy and the xuv intensity temporal profiles respectively, shown as solid lines in Figs.6(a) and (c). $W_i(t)$ is a simple function for $0 < t < 0.5$ fs with only one peak at $t = 0.20$ fs. $f_0(t)$ has a Gaussian-like shape centred at $t = 0.25$ fs, and its duration is 0.26 fs (FWHM), but it has a wider time span from 0 to 0.5 fs. Its area is normalized to 1. The excited Kr 4p photoelectrons are modulated by a dressing laser with a wavelength of $\lambda = 750$ nm, a duration of $\tau = 7$ fs (FWHM) and a carrier-envelope

phase of $\Phi = -30°$.

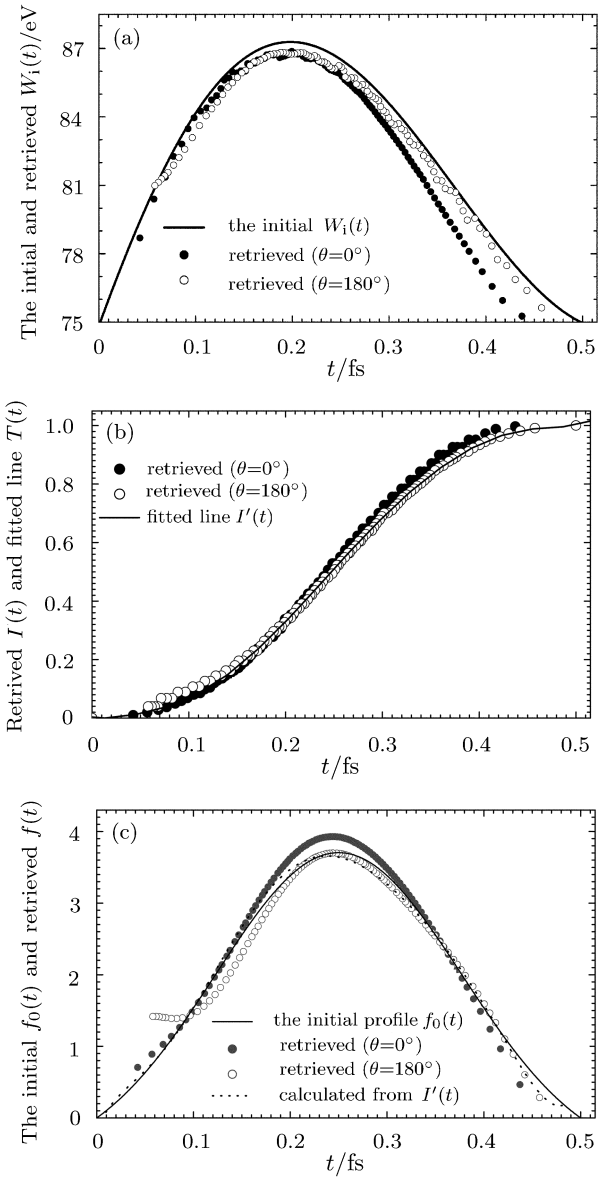


Fig.6. (a) The initial (solid line) and retrieved $W_i(t)$ (filled circles for $\theta = 0°$ measurement and open circles for $\theta = 180°$ measurement). (b) The energy-integrated spectra $I(t)$ (filled circles for $\theta = 0°$ measurement and open circles for $\theta = 180°$ measurement). The solid line $I'(t)$ is fitted from the combined data of filled circles and open circles. (c) The initial $f_0(t)$ (solid line) and the retrieved $f(t)$ (filled circles for $\theta = 0°$ measurement and open circles for $\theta = 180°$ measurement). The dotted line was calculated from $I'(t)$ in (b), its Gaussian fit $f(t) = -0.69 + 4.38\exp[-2(t-0.25)^2/0.26^2]$ is almost the same as $f_0(t) = -0.63 + 4.33\exp[-2(t-0.25)^2/0.26^2]$.

$n(W)$ at $\theta = 0°$ are calculated by using Eq.(4) with 1 eV energy bins at two laser intensities: $S_1 = 1 \times 10^{14}$ W/cm^2 and $S_2 = 2 \times 10^{14}$ W/cm^2. In this case, $W^{\rm H}_{0°}(t)$ is raised high enough to have almost no phase-overlapping. $n(W)$ is shown in Fig.3(b). The spectra $I(W)$ energy-integrated from $n(W)$ are also shown in Fig.3(b). Although $F(t-t_0)$ and $\sin\omega_{\rm L}t$ are two concurrent functions in two equations of Eqs.(7), t and $W_i(t)$ can be numerically determined by an iterating calculation. $W_i(t)$, $I(t)$ and the retrieved $f(t)$ are shown as filled circles in Fig.6(a), (b) and (c) respectively.

With above size of energy bins and laser intensities, the normalized spectra $n(W)$ and $I(W)$ are also calculated according to Eq.(5) for $\theta = 180°$ measurement. The retrieved $W_i(t)$, $I(t)$ and $f(t)$ are shown as open circles in Fig.6.

The combination of all data calculated for both $\theta = 0°$ and $180°$ measurements (filled and open circles) gives better reconstructions of $W_i(t)$ and $f(t)$. In Fig.6(b), the solid line $I'(t)$ is fitted from the combined data, its time derivative, $f(t) = {\rm d}I'(t)/{\rm d}t$, is shown as a dotted line in Fig.6(c). Its Gaussian fit, $f(t) = -0.69 + 4.38\exp[-2(t-0.25)^2/0.26^2]$, is almost the same as $f_0(t)$, i.e. the above calculation successfully reconstructs the initial intensity temporal profile $f_0(t)$.

3.2. Intensity temporal structure of a narrow bandwidth attosecond XUV

Assume that a $\hbar\omega_{\rm X} = 90$ eV (centre) and $\Delta W = 5$ eV bandwidth attosecond xuv is a train of four pulses ($f_0(t)$), as shown in Fig.7(a). Each pulse has a Gaussian intensity profile with a duration time of 150 as in FWHM. The pulses are separated by 300 as. The pulse with a higher peak is centred at $t = 0$ fs. The initial energy $W_i(t)$ of the photo-ionized Kr 4p electron is 76 eV. The energy spectrum $n(W)$ modulated by a $\tau = 7$ fs, $\Phi = -30°$ and $S = 4\times10^{13}$W/cm^2 laser is calculated according to Eq.(4) for $\theta = 0°$ measurement with 1 eV size of energy bins. The time t is calculated according to Eq.(12) for each energy position $W = W_{0°}$ of the spectrum $n(W)$. The derived temporal structure $f(t)$ is then calculated by using Eqs.(15) and (16) respectively.

In Fig.7(b), the solid line $f(t)$ is retrieved from the calculated $n(W)$ by using Eq.(15) with 1 eV size of energy bins. The error-bars are the temporal uncertainties at different times due to $\Delta W = 5$ eV xuv bandwidth. The plot shows that the intensity temporal structure is successfully reconstructed. Around $t = 0$ fs, the reconstruction has a higher time resolution than that at time point far from $t = 0$ fs. In Fig.7(c), the solid line, $f(t)$, is similar to that in

Fig.7(b), but it is retrieved with 2 eV size of energy bins. The dotted line is retrieved by using Eq.(16). For a time range of about a quarter of laser optical cycle around $t = 0$ fs, the results calculated by using Eqs.(15) and (16) are almost the same at current laser intensity.

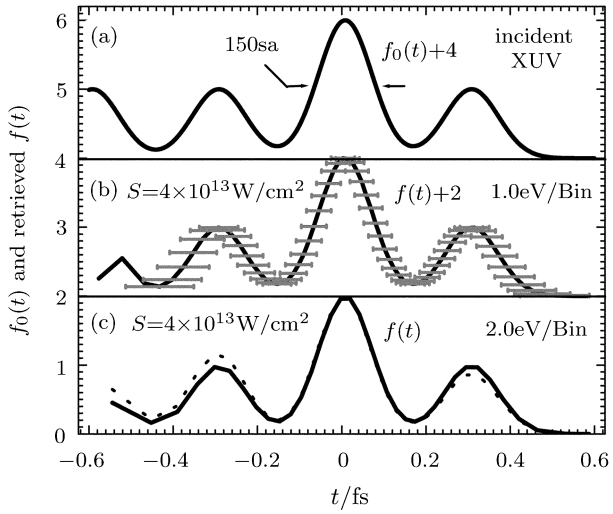


Fig.7. (a) The incident xuv. Its intensity temporal structure $f_0(t)$ contains four pulses, each of 150 as (FWHM) duration, and separated by 300 as. (b) The retrieved temporal structure $f(t)$ calculated by using Eq.(15) with 1 eV size of energy bins. The error-bar lengths at different times are the temporal uncertainties calculated by using Eq.(17) with $\Delta W = 5$ eV xuv bandwidth. (c) The retrieved temporal structures $f(t)$ calculated with 2 eV size of energy bins by using Eqs.(15) (solid line) and (16) (dotted line) respectively.

3.3. Intensity temporal structure of a narrow bandwidth femtosecond XUV

For $\theta = 90°$ femtosecond measurement, the energy spectra $n(W)$ and $\mathrm{d}n(W)/\mathrm{d}W$ are calculated according to Eq. (3). They are excited by a 600 fs train of $W_\mathrm{i} = 90$ eV (centre) xuv pulses, each of 15 fs (FWHM) duration, and separated by 30 fs. The photoelectrons are modulated by a $\tau = 100$ fs (FWHM), $\lambda = 750$ nm and $S = 4 \times 10^{13}$ W/cm^2 laser. The size of energy bins is 0.2 eV. Fig.8(a) shows the initial intensity structure $f_0(t)$ of the incident xuv, and the derived $f(t)$ with different laser wavelengths (532, 750 and 1064 nm) and sizes of energy bins (0.2, 0.2 and 0.6 eV) respectively. The bottom arrow points to t_M where a higher peak pulse is centred. Among the first three pulses of the incident xuv, only the first pulse centred at t_M is correctly retrieved for different laser wavelengths. The dotted lines in Fig.8(a) are shifted from $f_0(t)$. They are denoted as $k + f_0(t - t_\mathrm{d}) - A_\mathrm{d}$, where $k = 1, 2$ and 3 correspond to the laser wavelengths of 532, 750 and 1064 nm respectively. t_d is the time shift and A_d is the amplitude shift.

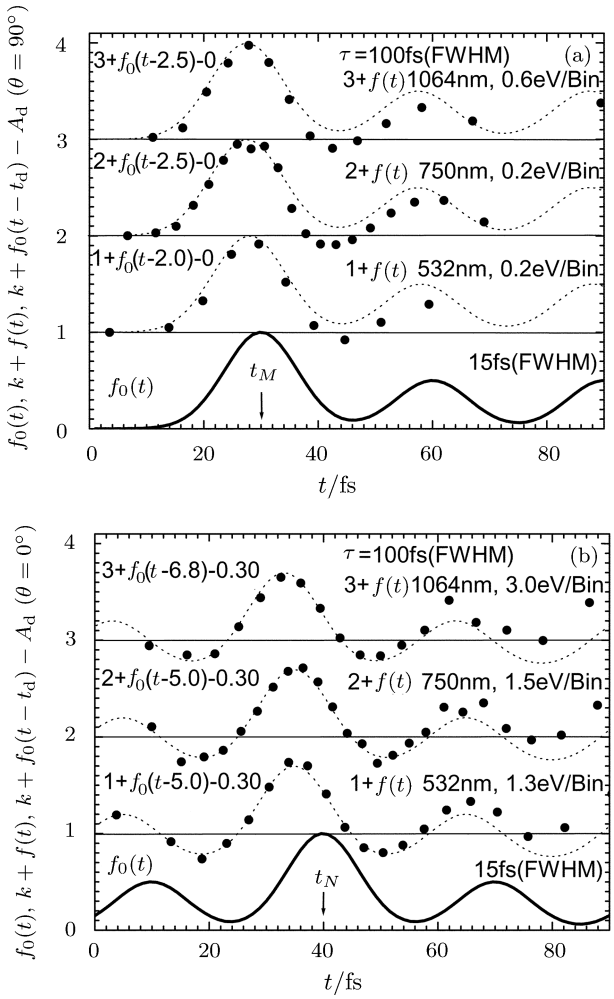


Fig.8. (a) $\theta = 90°$ measurements. The incident xuv intensity $f_0(t)$ (heavy solid line) and the retrieved $f(t)$ (filled circles) are shown. The dotted lines denoted as $k + f_0(t - t_\mathrm{d}) - A_\mathrm{d}$ ($k = 1, 2, 3$) are shifted from $f_0(t)$ for different laser wavelengths. (b) Similar to (a) for $\theta = 0°$ measurements.

With the same laser and xuv as in Fig.8(a), the energy spectrum $n(W)$ and $\mathrm{d}n(W)/\mathrm{d}W$ are calculated according to Eq.(4) at $\theta = 0°$. The size of energy bins is 1.5 eV. Fig.8(b) shows the intensity temporal structure $f_0(t)$ of the incident xuv and the retrieved $f(t)$ with different laser wavelengths (532, 750 and 1064 nm) and sizes of energy bins (1.3, 1.5 and 3.0 eV) respectively. The bottom arrow points to t_N where a higher peak pulse is centred. Among the first four pulses of the incident xuv, the second pulse centred at t_N for all three laser wavelengths are

successfully retrieved. For $\theta = 0°$ measurement, since the dynamic range of the photoelectron energy is much greater than that for $\theta = 90°$ measurement, the size of energy bins can be set to be a bigger one. In this case, obvious temporal and amplitude shifts of the retrieved $f(t)$ from the initial $f_0(t)$ are observed for different laser wavelengths. They are $t_{\rm d} = 5.0$, 5.0 and 6.8 fs for laser wavelengths 532, 750, 1064 nm, respectively. $A_{\rm d} = -0.30$ for all three different wavelengths. This is an interesting phenomenon of the transfer equations for $\theta = 0°$ measurement that needs further research.

Figure 9 shows the calculated temporal uncertainty Δt of the retrieved $f(t)$ corresponding to $\Delta W =$ 1 eV xuv bandwidth for $\theta = 0°$, $\lambda = 750$ nm, $S = 4\times10^{13}$ W/cm^2 and $\tau = 100$ to 500 fs (FWHM) lasers. The shaded areas illustrate the temporal ranges of feasible measurements for $\tau = 100$ and 400 fs (FWHM) lasers. The bottom arrow pointing to t_N denotes the minimum value of the function $\Delta t(t)$. The bottom arrow pointing to $t_{\rm R}$ denotes a recommended maximum value of the feasible measurement using a $\tau = 100$ fs laser, which is just the same as the t_N of the measurement using a $\tau = 200$ fs laser.

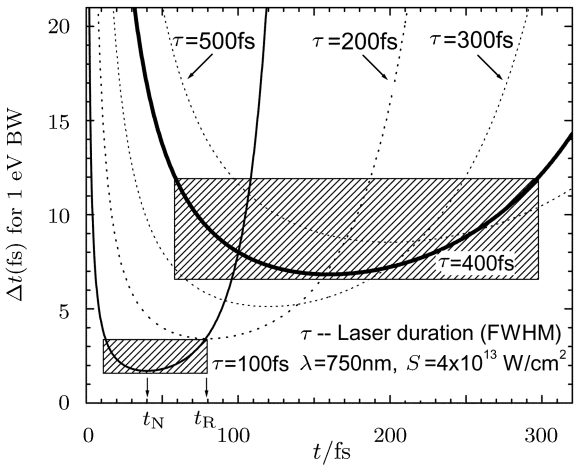


Fig.9. The temporal uncertainty Δt of the retrieved $f(t)$ calculated using Eq.(26) with $\Delta W = 1$ eV xuv bandwidth (BW).

4. Conclusion

For an attosecond xuv measurement, the pulse intensity and the instantaneous frequency can be retrieved from the energy-integral term of the PES by using a laser-phase determination method and a transfer equation. Two PES measurements are suggested with different laser intensities at $\theta = 0°$ or 180°. The appropriate laser intensities to be used depend on the temporal frequency profile of the incident xuv. The method has a temporal measurement range from a quarter to about half of the dressing laser optical cycle.

For a narrow bandwidth attosecond xuv measurement, the detailed temporal structure can be reconstructed from a proportional term of the PES. The method is a combination of using a laser-phase determination method and a transfer equation. The attosecond xuv should be located around or centred at $t = 0$ fs to obtain high time resolutions. The measurement range is about half of the dressing laser optical cycle. The temporal uncertainties at different times can be calculated with the value of the xuv bandwidth.

For a narrow bandwidth femtosecond xuv measurement, the following is a general procedure of measurement and calculation. Firstly, temporally locate the femtosecond xuv around t_M ($\theta = 90°$ measurement) or t_N ($\theta = 0°$ measurement). Secondly, measure PES with a high energy resolution spectrometer. Thirdly, calculate the PES with an appropriate size of energy bins, and derive the unknown temporal structure from an energy-differential term of the PES by using two transfer equations. These steps should be repeated to obtain higher time resolutions of the pulse retrieval. The $\theta = 0°$ measurement has higher time resolutions and a broader temporal measurement range than those of $\theta = 90°$ measurement, which depend on the intensity, wavelength and the duration of the dressing laser.

With presented laser-phase determination methods and transfer equations, the laser can be used as atto- and femtosecond rulers in ultrashort xuv or x-ray measurements.

Acknowledgments

The author gratefully acknowledges the support of Haiping He, and discussions with Y. L. Ye, D. X. Jiang and N. Z. Wu at Peking University, and B. S. Zhao at the Xi'an Institute of Optics and Precision Mechanics of Chinese Academy of Sciences.

References

[1] Drescher M, Hentschel M, Kienberger R, Tempea G, Spielmann C, Reider G A, Corkum P B and Krausz F 2001 *Science* **291** 1923

[2] Hentschel M, Kienberger R, Spielmann C, Reider G A, Milosevic N, Brabec T, Corkum P B, Heinzmann U, Drescher M and Krausz F 2001 *Nature* **414** 509

[3] Drescher M, Hentschel M, Kienberger R, Uiberacker M, Yakovlev V, Scrinzi A, Westerwalbesloh T, Kleineberg U, Heinzmann U and Krausz F 2002 *Nature* **419** 803

[4] Paul P M, Toma E S, Breger P, Mullot G, F. Balcou A P, Muller A G and Agostini P 2001 *Science* **292** 1689

[5] Constant E, Taranukhin V D, Stolow A and Corkum P B 1997 *Phys. Rev.* A **56** 3870

[6] Scrinzi A, Geissler M and Brabec T 2001 *Phys. Rev. Lett.* **86** 412

[7] Itatani J, Quéré F, Yudin G L, Ivanov M Y, Krausz F and Corkum P B 2002 *Phys. Rev. Lett.* **88** 173903

[8] Kitzler M, Milosevic N, Scrinzi A, Krausz F and Brabec T 2002 *Phys. Rev. Lett.* **88** 173904

[9] Band rauk A D, Chelkowski S and Shon N H 2003 *Phys. Rev.* A **68** 041802

[10] Quéré F, Itatani J, Yudin G L and Corkum P B 2003 *Phys. Rev. Lett.* **90** 073902

[11] Dinu L C, Muller H G, Kazamias S, Mullot G, Augé F, Balcou P, Paul P M, Kovačev M, Breger P and Agostini P 2003 *Phys. Rev. Lett.* **91** 063901

[12] Mairesse Y and Quéré F 2005 *Phys. Rev.* A **58** 3124

[13] Kienberger R, Goulielmakies E, Uiberacker M, Baltuska A, Yakovlev V, Bammer F, Scrinzi A, Westerwalbesloh T, Kleineberg U, Heinzmann U, Drescher M and Krausz F 2004 *Nature* **427** 817

[14] Goulielmakis E, Uiberacker M, Kienberger R, Baltuska A, Yakovlev V, Scrinzi A, Westerwalbesloh T, Kleineberg U, Heinzmann U, Drescher M and Krausz F 2004 *Science* **305** 1267

[15] Wang Z Y, Gong S Q and Xu Z K 1999 *Acta Phys. Sin.* **48** 961 (in Chinese)

[16] Zhou X X and Li B W 2001 *Acta Phys. Sin.* **50** 1902 (in Chinese)

[17] Wu J H and Yan J M 2003 *Chin. Phys.* **12** 1390

[18] Li P C, Zhou X X, Dong C Z and Zhao S F 2004 *Acta Phys. Sin.* **53** 750 (in Chinese)

[19] Bucksbaum P H and Merlin R 1999 *Solid State Commun.* **111** 535

[20] Lindenberg A M, Kang I, Johnson S L, Missalla T, Heimann P A, Chang Z, Larsson J, Bucksbaum P H, Kapteyn H C, Padmore H A, Lee R W, Wark J S and Falcone1 R W 2000 *Phys. Rev. Lett.* **84** 111

[21] Zholents A A and Zolotorev M S 1996 *Phys. Rev. Lett.* **76** 912

[22] Schoenlein R W and Leemans W P 1996 *Science* **274** 236

[23] Ge Y C, Li Y J and Kang K J 2005 *Acta Phys. Sin.* **54** 2669 (in Chinese)

[24] Ge Y C 2005 *Acta Phys. Sin.* **54** 2653 (in Chinese)

[25] Ge Y C 2006 *Acta Phys. Sin.* **55** 3386 (in Chinese)

[26] Dykhne A M and Yudin G L 1977 *Usp. Fiz. Nauk* **121** 157;
Dykhne A M and Yudin G L 1978 *Usp. Fiz. Nauk* **125** 377

[27] Gallagher T F 1988 *Phys. Rev. Lett.* **61** 2304

[28] Corkum P B, Burnett N H and Brunel F 1989 *Phys. Rev. Lett.* **62** 1259